PAPER

Transmission/absorption measurements for *in situ* monitoring of transparent conducting Ga:ZnO films grown *via* aqueous methods†

Moe Kevin and Ghim Wei Ho*

In this work, we devised a simple optical technique that allowed the nucleation and growth of Ga:ZnO films grown *via* aqueous synthesis at 90 °C to be studied *in situ*. Our two fold objective was to study the nucleation processes and to acquire real-time information of the film thickness. In doing so, the growth parameters (*e.g.* temperature, precursor concentration, and time) could be optimized to give the maximum yield, coupled with the ability to control the film thickness with a greater measure of precision and accuracy. We further demonstrated that such a degree of control could be used to fabricate transparent conducting electrodes of low sheet resistance (<10 Ω sq^{-1}) that meet the demands of photovoltaic applications. The electrical properties of the synthesized Ga:ZnO films and commercial Al:ZnO substrates showed comparable performance in dye-sensitized solar cells. This opened the possibility of a controlled low-cost aqueous route to fabricating high quality transparent conductor films that may well replace existing vacuum deposition techniques.

1. Introduction

Recent technological demand for thin films of ZnO in applications such as sensors, emission displays, photovoltaics, piezo-electronics, transparent conductors and solid-state lighting applications[1–10] has spurred the development of synthesis techniques based on low-temperature aqueous phase processes. Furthermore, flexible electronics that require films to be deposited on plastic substrates will likewise benefit from the low synthesis temperatures (<100 °C) that are maintained throughout the deposition process.

Aqueous phase deposition is also a vacuum-free process, thus negating the need for expensive vacuum pumps and chambers. Its scalability and environmental compatibility are also significant driving factors that have resulted in intense research into a variety of applications that represent established multi-billion dollar industries. Although aqueous phase deposition of films is often performed in many research laboratories, it remains difficult to precisely control and reproduce as the behavior of aqueous growth systems can vary significantly with parameters such as precursor concentrations, pH, reaction vessel geometry and heat capacity. Other forms of solution-based techniques such as sol–gel and chemical bath deposition also suffer from similar issues of reproducibility. Due to the stringent requirement of specific film thickness for certain

Department of Electrical and Computer Engineering, National University of Singapore, 4 Engineering Drive 3, 117576, Singapore. E-mail: elehgw@nus.edu.sg

† Electronic supplementary information (ESI) available. See DOI: 10.1039/c3ta12461d

applications, such as thickness characterization, post-growth cross-sectional and "stepped" planar samples are specially prepared for extensive film characterizations using expensive and time consuming techniques such as electron microscopy, ellipsometry, *etc.* The motivation for this work lies in that real-time knowledge of film nucleation and growth dynamics will be useful for applications where precise thickness is of key consideration. Characterization tools that provide such information like reflection high-energy electron diffraction (RHEED) have benefited molecular beam epitaxy (MBE) growth. However, the growth conditions and environment of aqueous phase deposition make it impossible to use any form of electron-based technique.

In this work, we demonstrate the use of an inexpensive, non-destructive optical technique to perform real-time monitoring of the nucleation and growth dynamics on Ga:ZnO films deposited using aqueous phase deposition, while enabling the nucleation temperature and film thicknesses to be determined *in situ* with accuracy. To the best of our knowledge, this is the first real-time observation of film growth and nucleation by the aqueous method. The optical technique uses no mechanical parts, which allows this method to become an inexpensive, sturdy and generic system for various aqueous methods at both the industrial and laboratory scale. This means that continuous-flow reactors, batch reactors and even microreactors will benefit as growth protocols can now be optimized to achieve the required growth conditions and film thicknesses, while minimizing wastage of precursors and time. Using this technique, we demonstrate the ease of optimizing the thickness of Ga:ZnO transparent conducting films for both low sheet resistance and

This journal is © The Royal Society of Chemistry 2013

J. Mater. Chem. A, 2013, **1**, 14239–14245 | **14239**

optimal transparency. As these films were intended to function as transparent conductors in photovoltaic devices, we fabricated dye-sensitized solar cells on our Ga:ZnO films and compared their performance with commercially available Al:ZnO substrates grown using vapour phase methods.

2. Experimental details

2.1. ZnO film deposition

ZnO nanoparticles were synthesized by adding a methanolic solution of KOH (15 ml, 0.41 M) to zinc acetate dihydrate (30 ml, 0.11 M) in a dropwise fashion at 60 °C. The solution was then capped and kept under constant stirring for 2 hours, during which the nanoparticles precipitated. The nanoparticles were then washed and dispersed in butanol. Glass or polyethylene terephthalate (PET) was first cleaned in DI water and isopropyl alcohol (IPA) for 3 min each and then spincoated on a substrate. The growth solution was prepared by adding aqueous ammonia (33%) to aqueous zinc nitrate in order to adjust the pH to 10.85. Trisodium citrate and gallium nitrate nonahydrate were added as the surfactant and dopant respectively. The substrate was then immersed face down in the growth solution and heated in a water bath at 70–90 °C for up to 8 hours.

2.2. Film characterization

SEM characterization was carried out using a JEOL FEG JSM 6700F field-emission scanning electron microscope operating at 15 keV with a built-in energy dispersive X-ray (EDX) attachment (Oxford Instruments and Inca software). TEM images were obtained using a JEOL-2100 high-resolution transmission electron microscope with an accelerating voltage of 200 keV. Sheet resistance measurements were carried out on 1×1 cm^2 samples (Van der Pauw configuration) at room temperature using a Keithley 4200 SCS. Photocurrent–voltage measurements for dye-sensitized solar cells were acquired using a AM1.5 solar simulator (Newport Instruments Model 91160A) with an AM filter (81088A). A 150 W Xe lamp was used as the illumination source. The light intensity corresponding to AM1.5 (100 mW cm^{-2}) was calibrated using a standard silicon solar cell (Oriel, SRC-1000-TC). A Maya2000 pro spectrometer (Ocean Optics) with a detection range of 200 nm < λ < 1100 nm was used to perform *in situ* optical transmission measurements. The spectrometer was set to record spectra at regular intervals to perform real-time observation.

3. Results and discussion

3.1. Film morphology

ZnO nanoparticles coated on the substrates served as nucleation sites for ZnO crystals that make up the film. These crystals occur in the form of nanowires due to anisotropic growth rates along the different crystallographic directions. ZnO has a wurtzite structure, and it is known that growth occurs the fastest in the $\langle 0002 \rangle$ c-direction, resulting in wire or pillar-like morphologies with the c-axis oriented in the out-of-plane direction. The morphology of the individual ZnO crystals can be tuned with the addition of surfactants and charged species.[11,12]

Fig. 1A summarizes the overall trends of crystal grain size and average film thickness as a function of trisodium citrate concentration. The role of trisodium citrate was to suppress the growth rate in the $\langle 0002 \rangle$ direction, while leaving the growth in the lateral $\langle 10-10 \rangle$ direction relatively unchanged by selective adsorption of citrate anions on the positively charged Zn-terminated (0002) plane.[11] This resulted in progressively thinner films and larger grain sizes as the concentration of citrate ions increased as indicated by the circular data points. Also from Fig. 1A, it is evident that the presence of Ga^{3+} ions (1.92 mM) contributed to the increase of the crystal grains as indicated by square data points. Thus gallium played a dual role as a dopant and served as a means of achieving a well coalesced film. The presence of Ga^{3+} did not significantly or systematically change the film thickness.

Fig. 1B–D show SEM images of ZnO crystals grown on glass substrates with 0, 0.62 and 1.86 mM of trisodium citrate respectively. With increasing concentrations of citrate ions, the nanowire array starts to exhibit a film-like structure across the entire substrate, albeit that at 1.86 mM of citrate, the film had not yet fully coalesced. Fig. 1E–G show Ga:ZnO crystals grown with 0, 0.62 and 1.86 mM of citrate ions just as before, but with the addition of 1.92 mM of gallium nitrate. It is clear that Ga doped films had larger grains and hence were better coalesced. Gallium incorporation was confirmed using EDX as shown in the ESI, Fig. S1.† Samples doped with 1.92 mM of Ga(NO$_3$)$_3$ had 1.3 at% gallium.

Full coalescence of films is essential for good electrical connectivity between grains, while a smooth surface without gaps is important to minimize light scattering. These two morphological attributes were fully met in the growth conditions used in Fig. 1G. Therefore, these conditions were used for the remainder of this study. The individual grains were highly oriented in the $\langle 0002 \rangle$ direction, giving the film a smooth surface with a root mean square roughness of 12 nm (see ESI Fig. S2† for XRD and AFM scans).

Cross-section TEM (Fig. 2A) revealed that films consisted of 3 distinct regions that are distinguished by crystal grain orientation and density. Within approximately 1 μm of the substrate, the film consisted of randomly oriented grains that consisted of crystals that grew from the randomly textured seed layer as seen in Fig. 2B. As the grains grew, they collided with each other to produce a region of spatially confined growth. This provided strong evidence that spatially-confined oriented growth[13] was the mechanism responsible for smooth film formation. The upper textured layer comprised highly c-axis oriented grains (Fig. 2C) that grew unhindered in the out-of-plane direction.

3.2. *In situ* monitoring setup

In order to monitor the nucleation and growth of Ga:ZnO films in real-time, we adopted the experimental setup as shown in Fig. 3. The setup essentially allows for standard optical transmission measurements to be performed during growth in real time using the spectrometer. This was possible since the Ga:ZnO films were grown on glass substrates, and the growth
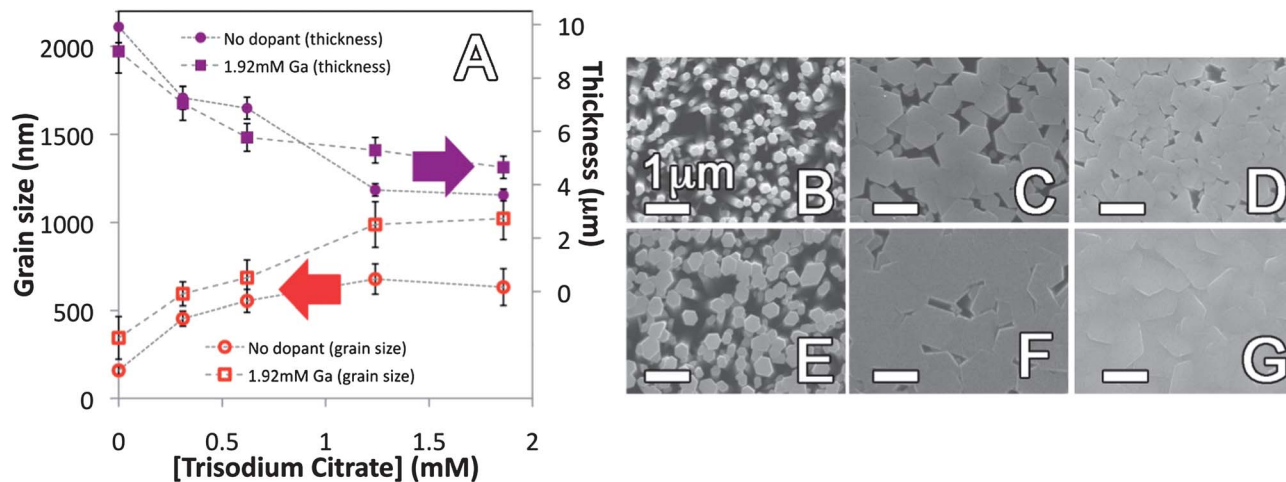
Fig. 1 (a) Plots of grain size (red) and film thickness (purple) as a function of citrate ion concentration; top-view SEM images of undoped films grown with (b) 0, (c) 0.62 and (d) 1.86 mM of trisodium citrate; top-view SEM images of films doped with 1.98 mM of Ga(NO₃)₃ grown with (e) 0, (f) 0.62 and (g) 1.86 mM of trisodium citrate.
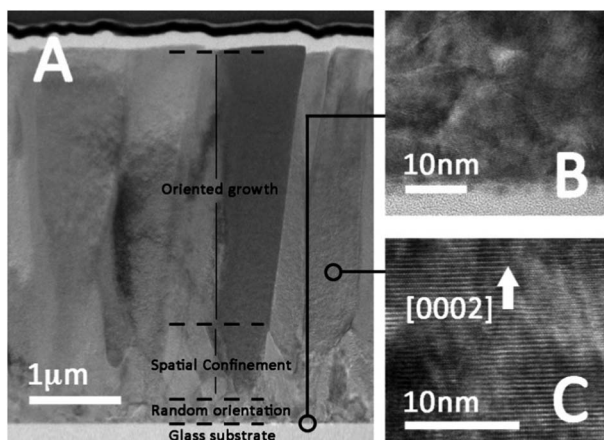

Fig. 2 (a) TEM cross-section of a Ga:ZnO film grown on glass. 3 distinctive layers have been identified as part of the spatially confined oriented growth model. (b) HRTEM image of the film–glass interface showing the nanoparticle seed layer and the randomly oriented grains of the film. (c) HRTEM image of the textured layer that consisted of highly oriented grains.
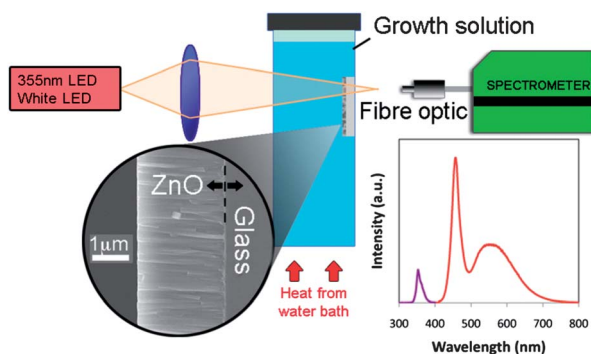

Fig. 3 Schematic setup of the optical technique used to perform *in situ* growth dynamics of the ZnO films. The inset spectrum shows the raw spectra of both the 355 nm LED and the white LED (∼420–700 nm).

itself was performed in a glass vial, all of which were transparent.

The light source consisted of a single homogenized beam of light from both a 355 nm UV light emitting diode (LED) and a broad spectrum white LED (∼420–700 nm). The beam was focused onto the seeded glass substrate when immersed in the growth solution, while a fiber optic cable was used to collect the light from the opposite side of the substrate. The intensity was periodically measured using the spectrometer at 1 min intervals. The inset of Fig. 3 shows the raw spectrum from both the UV and white LEDs.

Light from the 355 nm LED was easily absorbed by ZnO as it has energy well above the bandgap (∼3.37 eV; ∼368 nm). The purpose of the 355 nm UV light was to detect the onset of ZnO secondary nucleation on the substrate as its intensity was sensitive to ZnO films of sub-50 nm thicknesses. The broad spectrum white LED provided a steady source of light from 420–700 nm that was used to construct a transmission spectrum at regular time intervals using

$$\text{Tr}(t) = I_t/I_{t=0}$$

where $\text{Tr}(t)$ is the transmission spectrum as a function of time. $\text{Tr}(t)$ was calculated from the ratio of the intensity measured at time t (I_t) and the initial intensity at the start ($I_{t=0}$). As the Ga:ZnO film grew, interference between the film and the substrate gave rise to oscillations in the transmission spectra. By noting the peak positions of the oscillations in the spectra, the thickness of the film can be calculated using the relation as obtained by Swanepoel[14]

$$D = \lambda_1\lambda_2/2(n_1\lambda_2 - n_2\lambda_1)$$

where D is the thickness of the film in nanometers; λ_1 and λ_2 are the wavelengths of any two consecutive peaks or troughs in the transmission spectra, and n_1 and n_2 are the corresponding refractive indexes of ZnO at λ_1 and λ_2. The

This journal is © The Royal Society of Chemistry 2013

J. Mater. Chem. A, 2013, **1**, 14239–14245 | **14241**

refractive indexes were obtained from the first-order Sellmeier equation:

$$n(\lambda)^2 = A + B\lambda^2/(\lambda^2 - C^2)$$

with fitting parameters $A = 2.84$, $B = 0.84$ and $C = 0.319$ μm.[15] Our approach was to consider several consecutive pairs of peaks to obtain an average value of D. The principle behind the oscillations is the constructive and destructive interference of reflected light that originates from the film surface and the film–glass interface.

Thicker films gave rise to transmission spectra with more oscillations. Fig. 4A shows the oscillations of 2 transmission spectra: the sample with more peaks (represented by the black solid line) was 2.53 μm thick, while the sample with fewer peaks (dashed blue line) was 0.93 μm thick. This places a lower limit on the film thickness that can be measured as films thinner than 500 nm would not manifest at least 2 peaks within the range of 420 nm< λ < 680 nm. One way around this problem would be to extend the range of the illuminating LEDs to include near-IR wavelengths. Fig. 4B shows the reliability of this technique by comparing 20 different film thicknesses obtained

Fig. 4 (a) Characteristic oscillations from the transmission spectra of 2.53 μm and 0.93 μm films. (b) A plot of film thicknesses as measured using the Swanepeol technique (vertical axis) and from cross-section SEM (horizontal axis).

from both SEM cross-sections and the Swanepoel method, showing strong agreement between both measurements.

3.3. Determining temperatures for homogeneous and secondary nucleation

In this section, we discuss the usage of the optical technique to determine the secondary and homogeneous nucleation temperatures. Growth solutions consisting of a zinc salt and ammonia in an aqueous solution are known to exhibit retrograde solubility[16] i.e. elevated temperatures in the range of 70–90 °C are required to supersaturate the system in order for ZnO crystals to grow.

For this discussion, the nucleation temperature (T_n) is the minimum temperature required for secondary growth to occur. Here, secondary growth is defined as the formation of a new ZnO material on an existing ZnO crystal. Below T_n, no growth occurs. At temperatures equal to or slightly larger than T_n, only secondary growth is favourable. Under these conditions, ZnO grows on surfaces that have been pre-coated with ZnO nanoparticles. At a higher temperature T_{hom}, homogeneous nucleation becomes favourable, resulting in uncontrolled precipitation of ZnO crystals in the solution phase. This causes the growth vessel to become cloudy, and precipitates can potentially contaminate the substrate surface. More importantly, ZnO precipitates compete with film growth for zinc nutrients, resulting in much wastage of precursors. Therefore, it is highly desirable to perform growth at a temperature (T_{growth}) where $T_n \leq T_{growth} \ll T_{hom}$, in order to provide a sufficiently high supersaturation to drive secondary growth, while suppressing homogeneous nucleation.

As it is nearly impossible to predict T_n based on the growth parameters (e.g. zinc nitrate concentration, pH, and concentration of dopants/surfactants), we sought to determine T_n experimentally by using the optical technique described above.

T_n and T_{hom} were obtained using the experimental setup shown in Fig. 3. The strategy was to ramp the temperature from well below the vicinity of T_n at a rate of 0.5 °C min^{-1}, until a drop in the 355 nm intensity was detected. This drop represented the onset of secondary nucleation of Ga:ZnO on the substrate. All other wavelengths >400 nm still maintained their intensities as Ga:ZnO is transparent to visible light. The temperature was then further increased until homogeneous nucleation occurred. This caused the solution to turn cloudy, resulting in a drop in the transmission across all visible wavelengths. Fig. 5A shows the results from a solution prepared with 32.5 mM zinc nitrate. The 355 nm intensity dropped at approximately 60 min in the experiment when the temperature was ~82 °C. When the temperature was subsequently increased, the visible light transmission (represented by $\lambda = 550$ nm) started to decrease at ~89 °C due to homogeneous nucleation of ZnO precipitates. Using this technique, both T_n and T_{hom} could be determined with a greater measure of accuracy.

Fig. 5B shows the results of a series of experiments performed in a similar manner, using zinc nitrate concentrations that ranged from 6.25 mM to 50 mM while keeping the pH constant at 10.85. It showed that T_n and T_{hom} not only increased
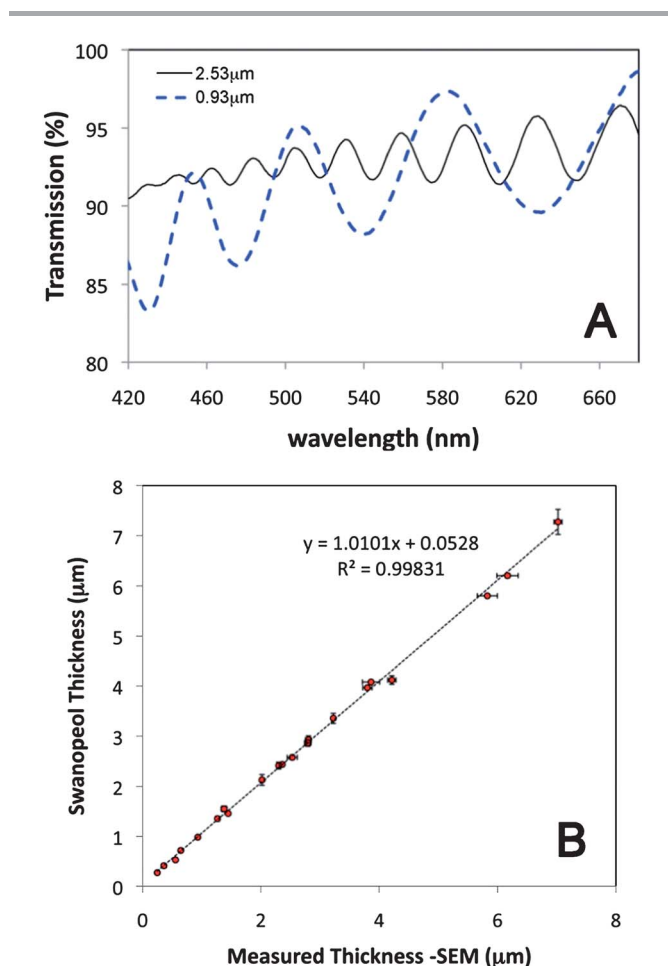
14242 | J. Mater. Chem. A, 2013, **1**, 14239–14245

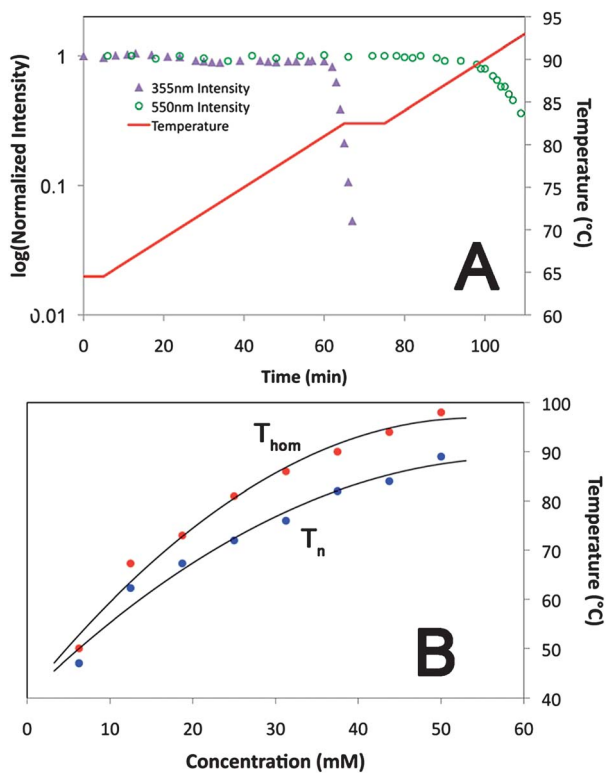This journal is © The Royal Society of Chemistry 2013

Fig. 5 (a) The log(normalized) transmission at 355 nm (triangles) and 550 nm (open circles) is measured as a function of time as light passed through the substrate during growth. Temperature (solid line) is slowly ramped until the onset of nucleation as indicated by the sudden drop in 355 nm transmission. Further increase in temperature made homogeneous nucleation favourable, triggering the drop in 550 nm transmission. (b) A plot of measured T_n and T_{hom} as a function of zinc nitrate concentration.

with zinc nitrate concentration, but also with relative difference between T_n and T_{hom}. To explain this, we note that more ammonia was required to achieve a pH of 10.85 when zinc nitrate was present in higher concentrations. We postulate that more ammonia caused the zinc species to be more soluble through the formation of the zinc tetra-amine complex.[16] Consequently, higher temperatures were required to provide sufficient supersaturation for growth. It is worth noting that aqueous systems with higher zinc nitrate concentrations have a larger temperature window ($T_{hom} - T_n$) for secondary growth, making temperature control less of a problem.

Having obtained knowledge of T_n and T_{hom} over a range of zinc nitrate concentrations, we proceeded to grow Ga:ZnO with 25 mM (estimated $T_n \sim 71$ °C) of zinc nitrate. Fig. 6A shows the temperature profile rising to 77 °C within 9 min. Nucleation occurred within 4 min when the temperature reached 72 °C as indicated by the drop in the 355 nm intensity. This is in good agreement with the previously determined T_n value. About 12 min after nucleation, the first pair of peaks in the visible spectra appeared. The real-time film thickness determined using the Swanepoel method is indicated by the black squares. A backward linear extrapolation of the black squares onto the time-axis coincides with the onset of secondary growth, confirming that the nucleation and thickness measurements are consistent with each other.

Thus far, we have shown that T_n and T_{hom} could be determined in real time for the growth systems described here. Such knowledge was useful for suppressing the formation of precipitates, while ensuring that the growth systems were sufficiently supersaturated for growth.

3.4. Monitoring film thickness

In this section, the Swanepoel method was used to monitor the film thickness over the span of 5 hours for different growth temperatures. Fig. 6B shows the thickness of Ga:ZnO films in real-time, grown using 25 mM zinc nitrate growth solutions ($T_n \sim 70$ °C, $T_{hom} \sim 80$ °C). Each curve represents growth performed at a specific temperature. At the nucleation temperature of 70 °C, growth proceeded slowly at a rate of approximately 2 μm h^{-1} and did not cease within the 5 hour time span. This is attributed to the relatively low level of supersaturation as the growth temperature was very close to the nucleation temperature. At 75 °C, the initial growth rate increased to about 3.6 μm h^{-1} because of the increased supersaturation. However, while no homogeneous precipitates were formed, we observed nucleation of Ga:ZnO on the vessel wall, reducing the amount of zinc nutrients that reach the substrate. This explains why the final thickness of the film at 75 °C was thinner than the film grown at 70 °C. At higher temperatures (80–90 °C), homogeneous nucleation occurred, causing the films to stop growing within the 5 hour time span. Higher temperatures caused more precipitates to form, resulting in less growth of the film. The results of this experiment confirmed that our strategy of performing growth close to the nucleation temperature will produce the greatest film yield. As shown here, the optimum growth temperature lies within a 5 °C window which poses a challenge for controlling film growth. However as demonstrated in Fig. 5B, this optimum window can be made larger by increasing zinc nitrate concentration, keeping other variables constant.

Fig. 6B and C show film thicknesses grown from growth solutions that contained 31.25 mM ($T_n \sim 75$ °C, $T_{hom} \sim 87$ °C) and 43.75 mM ($T_n \sim 81$ °C, $T_{hom} \sim 95$ °C) of zinc nitrate. At a zinc nitrate concentration of 31.25 mM, no growth occurred at 70 °C as it was below the nucleation temperature. At 75–80 °C, the film thicknesses did not saturate within the 5 hour time span, and no nucleation on the vessel wall was observed. This indicated that secondary growth on the seeded substrate dominated within this temperature range, making this temperature range ideal for growth. This was further supported by the fact that the maximum film growth was achieved at 80 °C (7.8 μm). Subsequently higher temperatures (85–90 °C) exhibited homogeneous nucleation that limited the maximum thickness of the films. A similar trend was observed for growth with 43.75 mM of zinc nitrate with the ideal temperature being approximately 90 °C, giving a maximum thickness of 9.8 μm. Therefore, zinc nitrate concentration can function both as a variable to tune the growth solution's optimum temperature window, and to increase the maximum obtainable film thickness.
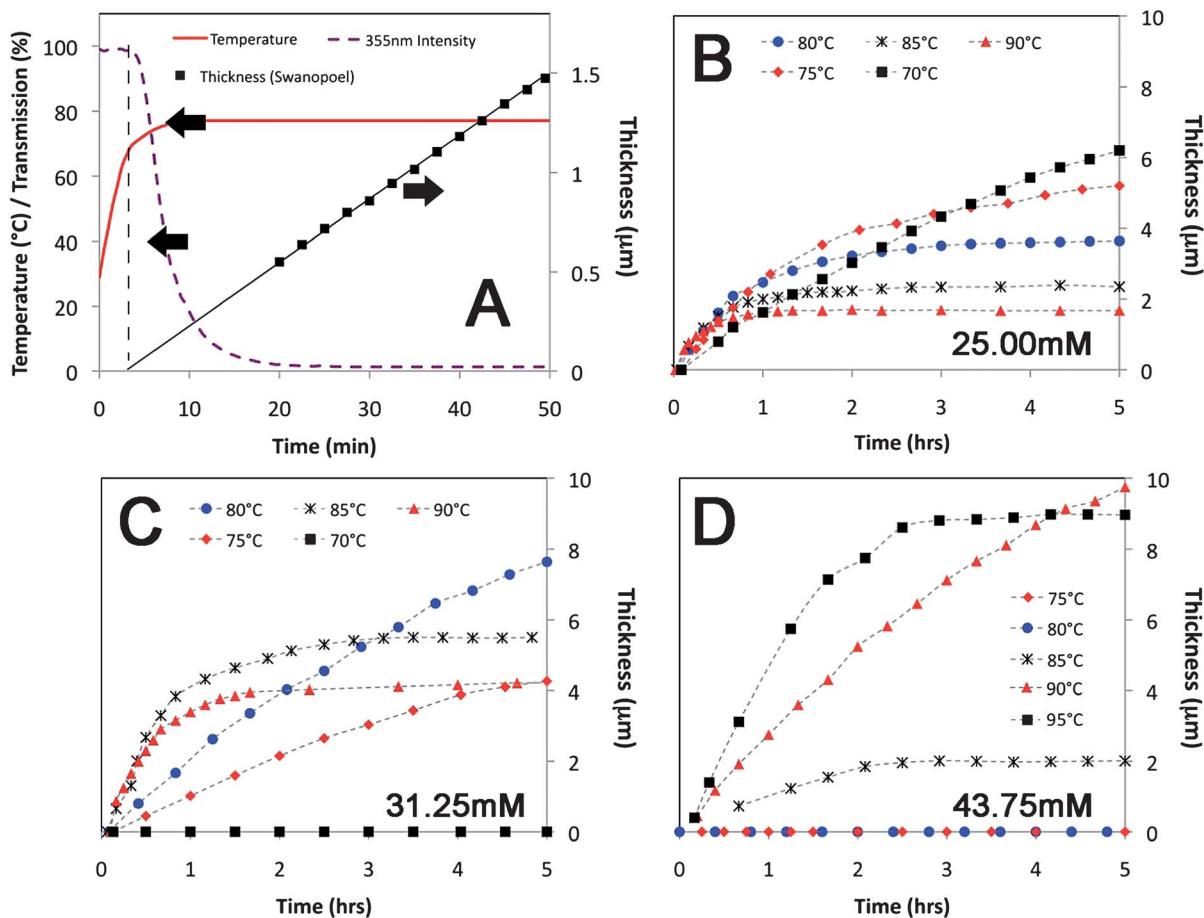
Fig. 6 (a) 355 nm transmission intensity and temperature as a function of time. The growth system was placed directly in a pre-heated water bath. Black squares indicate film thickness measured using the Swanepoel method as soon as 2 peaks were visible. (b–d) Films thicknesses as a function of time at different growth temperatures. Solutions contained (b) 25 mM (c) 31.25 mM and (d) 43.75 mM of zinc nitrate at a pH of 10.85 with 1.86 mM trisodium citrate and 1.92 mM gallium nitrate.

It is interesting to note that while mild levels of side wall nucleation or homogeneous nucleation might attenuate the transmission spectra, they did not interfere with the real-time Swanepoel measurements because the relative positions of the oscillation peaks remain unchanged by the random scattering of light from the precipitates. This made the technique sufficiently robust to perform in aqueous environments.

3.5. Optimizing film thickness for solar cells

The potential of the technique is best appreciated when it is used to monitor the growth of transparent conducting films for photovoltaic applications, where a low sheet resistivity ($\sim$10 Ω sq^{-1}) is required. All Ga:ZnO films were annealed at 350 °C for 30 min in a muffled furnace before sheet resistance measurements were performed. This was to activate the dopant atoms as demonstrated in a previous study.[17] Since sheet resistance is strongly dependent on the film thickness, we studied this dependence by growing several films to different thicknesses using the growth system's optimum temperature, and plotting their corresponding sheet resistances in Fig. 7A. It was

determined that sheet resistances of <10 Ω sq^{-1} were obtained when films were at least 6.4 μm.

In order to show the effects of sheet resistance on solar cell performance, three Ga:ZnO films were grown to 6.4 μm, 4.5 μm and 3.8 μm with sheet resistances of 9, 24 and 46 Ω sq^{-1} respectively. Dye-sensitized solar cells were fabricated by doctor-blading commercial ZnO nanoparticles onto the Ga:ZnO films as described elsewhere.[17] For comparison, a similar device was fabricated using a commercial Al:ZnO (10 Ω sq^{-1}) substrate. The J–V characteristics are plotted in Fig. 7B. The 9 Ω sq^{-1} Ga:ZnO device had an efficiency of 3.29%, which was comparable to the commercial Al:ZnO device (3.37%). This difference in efficiency was due to the lower photocurrent produced as shown in Fig. 7B. This in turn is attributed to a slightly lower transparency of the Ga:ZnO substrate as shown in the transmission spectra in the ESI Fig. S3.† As the sheet resistance increased, the corresponding efficiencies decreased to 2.80% and 2.08% for Ga:ZnO sheet resistances of 24 Ω sq^{-1} and 46 Ω sq^{-1} respectively. This was due to resistive losses in the transparent conducting substrate. This demonstrated that if Ga:ZnO films are sufficiently thick, they have the potential to rival commercially available transparent conductors deposited by
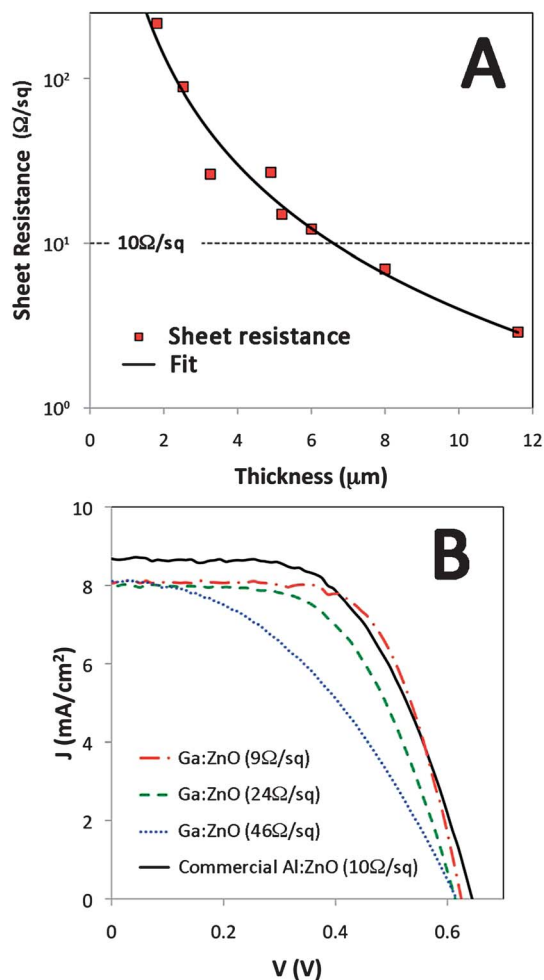
Fig. 7 (a) A plot of sheet resistance against Ga:ZnO thickness. The 10 Ω sq^{-1} mark is denoted by the horizontal dotted line, and it corresponds to a thickness of 6.4 mm. (b) J–V curves of dye-sensitized solar cells fabricated on transparent conducting substrates of different sheet resistances.

vacuum methods. Hence, the ability to obtain real-time information about the film thicknesses is essential from the perspectives of both device performance and the fabrication process.

4. Conclusion

Nucleation and growth of Ga:ZnO transparent conducting films on glass substrates were studied *in situ* using a simple integrated optical technique. The onset of secondary nucleation was detected by the absorption of 355 nm UV light, while the *in situ* measurement of film thickness was measured using the Swanepoel method. Using the technique, we showed that the temperature window of optimum growth became larger as the zinc precursor concentration was increased. This was between the temperatures associated with the onset of secondary growth

and homogeneous nucleation. This provided a simple route towards the reproducible fabrication of films that can now be easily controlled in real-time. Using the real-time measurements of film thickness, transparent conducting films were fabricated to the minimum required thickness for achieving a sheet resistance of 10 Ω sq^{-1}. Dye-sensitized solar cells were subsequently fabricated on Ga:ZnO films and efficiencies were comparable to devices fabricated using commercial transparent conductors. We believe that this optical approach to study nucleation and growth of Ga:ZnO films has the potential to become an indispensable tool for monitoring industrial-scale growth that suits batch or continuous flow reactor configurations.

Acknowledgements

References

1 F. Ye, X. M. Cai, F. P. Dai, D. P. Zhang, P. Fan and L. J. Liu, *Phys. B*, 2012, **407**, 64–67.
2 H. Akazawa, *J. Vac. Sci. Technol., A*, 2011, **29**, 031304.
3 B. Y. Oh, J. H. Kim, J. W. Han, D. S. Seo, H. S. Jang, H. J. Choi, S. H. Baek, J. H. Kim, G. S. Heo, T. W. Kim and K. Y. Kim, *Curr. Appl. Phys.*, 2012, **12**, 273–279.
4 P. P. Sahay, *J. Mater. Sci.*, 2005, **40**, 4383–4385.
5 M. Suchea, S. Christoulakis, K. Moschovis, N. Katsarakis and G. Kiriakidis, *Thin Solid Films*, 2006, **515**, 551–554.
6 R. C. Lin, Y. C. Chen and K. S. Kao, *Appl. Phys. A: Mater. Sci. Process.*, 2007, **89**, 475–479.
7 J. B. Lee, H. J. Kim, S. G. Kim, C. S. Hwang, S. H. Hong, Y. H. Shin and N. H. Lee, *Thin Solid Films*, 2003, **435**, 179–185.
8 Z. L. Wang and J. H. song, *Science*, 2006, **312**, 242–246.
9 A. K. K. Kyaw, X. W. Sun and C. Y. Jiang, *J. Sol-gel Sci. Technol.*, 2009, **52**, 348–355.
10 L. L. Chen and C. C. Huang, *Nanoscale Res. Lett.*, 2012, **7**, 627.
11 S. Cho, J.-W. Jang, S.-H. Jung, B. R. Lee, E. Oh and K.-H. Lee, *Langmuir*, 2009, **25**, 3825.
12 J. Joo, B. Y. Chow, M. Prakash, E. S. Boyden and J. M. Jacobson, *Nat. Mater.*, 2011, **10**, 596–601.
13 M. Podlogar, J. J. Richardson, D. Vengust, N. Daneu, Z. Samardžija, S. Bernik and A. Rečnik, *Adv. Funct. Mater.*, 2012, **22**, 3136–3145.
14 R. Swanepoel, *J. Phys. E: Sci. Instrum.*, 1983, **16**, 1214.
15 W. L. Bond, *J. Appl. Phys.*, 1965, **36**, 1674.
16 J. J. Richardson and F. F. Lange, *Cryst. Growth Des.*, 2009, **9**(6), 2570–2575.
17 M. Kevin, G. H. Lee and G. W. Ho, *Energy Environ. Sci.*, 2012, **5**, 7196–7202.

This journal is © The Royal Society of Chemistry 2013

J. Mater. Chem. A, 2013, **1**, 14239–14245 | **14245**